Identification of different pathways of electron injection in dye-sensitised solar cells of electrodeposited ZnO using an indoline sensitiser†

Iulia Minda,*[a] Essraa Ahmed,[a] Vivien Sleziona,[a] Christoph Richter,[b] Max Beu,[b] Jane Falgenhauer,[b] Hidetoshi Miura,[c] Derck Schlettwein[b] and Heinrich Schwoerer[a]

Charge transfer dynamics in fully operational dye sensitised solar cells consisting of an electrolyte or organic spiroOMeTAD in contact with a highly porous electrodeposited ZnO film sensitised with a monolayer of the indoline dye DN216 were observed using ultrafast transient absorption spectroscopy. From the temporal evolution of spectral signatures assigned with the help of spectroelectrochemical experiments to the population and depopulation of initial, transient and final states, a model was completed for the multistep injection of photoexcited electrons from the molecular absorber to the ZnO acceptor. Injection was found to occur *via* three different paths with three characteristic rates: directly from the dye's lowest unoccupied molecular orbital into the ZnO conduction band (200 fs) and *via* intermediate molecular dominated and surface dominated hybrid states (2 ps and 10 ps, respectively).

1 Introduction

The contribution of photovoltaics as a renewable energy source to the world's electricity generation will increase in the next few decades. In contrast to coal, gas or nuclear power stations, photovoltaic units are independent of an electricity grid and fuel supply and are almost infinitely down scalable, thus qualifying photovoltaics for application in remote areas and developing environments. Even if classified as a supplementary technology, it needs to be realistically sustainable, meaning that the energy payback time of devices must be much shorter than their operating lifetime, demanding optimisation of cost, energy of fabrication, efficiency and durability. This multi-parameter range offers potential for photovoltaic devices based on organic absorbers such as dye sensitised solar cells, as reported in this paper, copolymer and bulk heterojunction cells and even hybrid organic/inorganic perovskite solar cells. They largely consist of harmless elements abundant in the earth's crust (except the currently still lead containing perovskites). Organic solar cells were developed as promising alternatives to the market dominating silicon solar cells. They can be fabricated by simple low temperature methods such as electrodeposition,

spin coating or even printing on polymer foils.[1–3] These flexible substrates together with the variability of organic molecules and their absorption wavelength regions even offer appealing design options.

Efficient dye sensitised solar cells (DSSCs) consist of a monolayer of organic absorber molecules adsorbed onto a nanoporous semiconductor surface. Even though a monolayer of dye is used, high absorptivity is maintained due to the increased surface area of the highly porous semiconductor. Moreover, the photoexcited dye molecules are located on the semiconductor surface, thus eliminating exciton propagation dynamics. The field of DSSCs has progressed since the pioneering devices reported by Grätzel and O'Regan,[4] from ruthenium based dyes adsorbed onto a highly porous TiO_2 structure, to various organic and inorganic absorbers[5–9] and different electron and hole accepting materials.[3,5,10–16] To date, the highest achieved certified efficiency of a DSSC is 11.9%,[17] although cells with efficiencies of up to 13% and 14% have also been reported.[18,19] DSSCs, produced with ZnO rather than TiO_2 as the electron accepting semiconductor, are less efficient despite a higher electron mobility of ZnO and, hence, decreased transport resistance in DSSCs.[20–26] Differences in injection dynamics are often held responsible for the decreased efficiency,[25] however, highly porous ZnO films can be electrodeposited at low temperatures ($\sim 70\ ^\circ C$) in contrast to the high temperature ($\sim 450\ ^\circ C$) annealing process required for the TiO_2 films, thereby allowing the ZnO devices to be manufactured on flexible substrates and at even lower cost, reducing the energy payback time further.[22,27–30] A notable distinction to TiO_2 is

[a] *Laser Research Institute, Stellenbosch University, Stellenbosch, South Africa. E-mail: heso@sun.ac.za; Fax: +27 21 808 3385; Tel: +27 21 808 3375*

[b] *Institut für Angewandte Physik, Justus-Liebig-Universität, Heinrich-Buff-Ring 16, 35392 Giessen, Germany*

[c] *Chemicrea Co., Ltd., 2-1-6 Sengen, Tsukuba, Ibaraki 305-0047, Japan*

† Electronic supplementary information (ESI) available. See DOI: 10.1039/c5cp07841e

8938 | *Phys. Chem. Chem. Phys.,* 2016, **18**, 8938–8944

This journal is © the Owner Societies 2016

that electrodeposited highly porous ZnO films contain trap states in the bulk of the films and at their surface which play a decisive role in recombination reactions, as well as in the electron injection process from the absorbing dye to the ZnO acceptor. In a number of time resolved experimental studies on indoline dye sensitised cells, multiexponential dynamics of the excited and oxidised dye have also been reported pointing to different injection channels.[23,24,31,32] However, none of these experiments have directly measured the ultrafast population of the ZnO conduction band. Furube *et al.*[33,34] have observed electron injection dynamics in N3 dyes adsorbed to sintered ZnO, which were explained as injection *via* different charge transfer states.

In this report we describe the initial photoinduced charge separation in indoline dye sensitised electrodeposited ZnO solar cells, being interesting and promising candidates for both the study of the fundamental photophysics of light harvesting as well as real power generation.

Conventional electrochemical characterisation in combination with steady state spectroscopy of solar cell devices by means of *I–V* dependence, impedance spectroscopy, and external and internal quantum efficiency measurements provides detailed and standardised measurements of the cell's light to electric power conversion efficiency, durability and macroscopic performance. Elaborating further, ultrafast spectroscopy allows for the observation of the initial interaction of light with the absorbing molecular unit, the subsequent dynamics of the excitation and separation of charges and eventually their injection and propagation into the electron and hole conduction species in a particular cell. We use femtosecond transient absorption spectroscopy (TAS), observing the evolution of characteristic spectral signatures in time, which are attributable to particular charge and energy states in the device. This microscopic view reveals the basic physics and chemistry reasons for the efficiency of a solar cell and is therefore helpful for material, processing and architecture design optimisation.

We have previously reported on charge transfer processes in fully operational indoline/electrodeposited ZnO solar cells. Spectroscopic signatures in the visible regime allowed us to monitor the different transient states of the dye.[35,36] Here we extend such TAS measurements to the IR regime, which enables the direct observation of the stepwise electron injection into the ZnO conduction band *via* intermediate charge transfer states. The experiments identified three main charge injection channels from the photoexcited dye to the electron accepting semiconductor ZnO, and lead us to the formulation of a complete photoexcitation, charge separation and charge injection model of the indoline sensitised electrodeposited ZnO solar cell.

2 Experimental details and procedures

2.1 Sample preparation

Our study was carried out on fully operational sandwich cells made by the sensitisation of a nanoporous electrodeposited ZnO electron accepting layer with a monolayer of the organic indoline dye DN216. The circuits were closed with either a conventional iodide/triiodide redox couple in electrolyte solution as described earlier[36] or with a solid hole conductor by spin coating 40 μL of a solution consisting of 180 mg mL^{-1} of 2,2′,7,7′-tetrakis-(*N,N*-di-*p*-methoxyphenyl-amine)-9,9′-spiro-bifluorene (spiroOMeTAD, Borun Chemicals 99.75%), 6.4 mg mL^{-1} of lithium bis(trifluoromethanesulfonyl)imide (Li-TFSI, Sigma-Aldrich, 99.5%), 30 mg mL^{-1} of acetonitrile (Roth, 99.9%) and 16 mg mL^{-1} of *tert*-butylpyridine (Sigma-Aldrich, 99%) in chlorobenzene (Roth, 99.5%) at 3000 rpm for 30 s and finalised by an evaporated 100 nm silver (Sigma-Aldrich 99 999%) counter contact. The devices were optimised for optical transmittance, which has to be measured using ultrafast TAS, rather than for maximum efficiency, which was accomplished by reducing the dye deposition time.

2.2 Femtosecond transient absorption

Fully operational solar cells were measured by femtosecond transient absorption spectroscopy in a pump–probe setup. It consists of a ClarkMXR CPA2101 amplified titanium:sapphire laser, pumping two non-colinear optical parametric amplifiers (NOPA) operating in the visible or near infrared spectral range, and a white light continuum source (WLC). The NOPAs deliver near transform limited pulses of sub 50 fs duration in the wavelength ranges of 450–700 nm and 900–2800 nm. The WLC covers 350–1400 nm using CaF$_2$, sapphire and YAG crystals. The chirp corrected duration of the uncompressed WLC pulses is limited to approximately 150 fs by the duration of the CPA laser pulses.

One of the NOPA pulses serves as the solar cell exciting pump pulse with its central wavelength set to the steady state absorption maximum of the cell ($\lambda_{\max}$ = 530 nm).[36] Upon recording the sample's absorption spectrum in the visible and infrared spectral regime, the change in optical density is determined $\Delta OD(\lambda) = \ln(I_p(\lambda)/I_0(\lambda))$, where $I_p(\lambda)$ is the transmission spectrum of the excited sample and $I_0(\lambda)$ is the transmission spectrum of a nonexcited sample as reference. $\Delta OD(\lambda)$ is measured for different time delays t between the pump and probe pulses set using a micromechanical linear translation stage in one of the beams. Depending on the choice of probe pulse source the overall temporal resolution of the TAS setup is sub 100 fs (NOPA–NOPA) or sub 160 fs (NOPA–WLC). The probe light pulses are spectrally dispersed in two spectrometers (ANDOR SR150) and detected using two line scan cameras sensitive in the visible and near infrared range up to 2500 nm, respectively (Ingenieurbüro Stresing, Berlin, Germany). Single pulse detection at 1 kHz repetition rate and chopper modulation of every second pump pulse allows for a pulse to pulse reference measurement of excited and nonexcited samples, resulting in an optical density sensitivity of $\Delta OD \leq 5 \times 10^{-4}$.

2.3 Experimental procedure

Transient absorption spectra were measured for various spectral regions between 400 nm and 2400 nm, a selection of which is shown in Fig. 1. Sections a and b were recorded using an
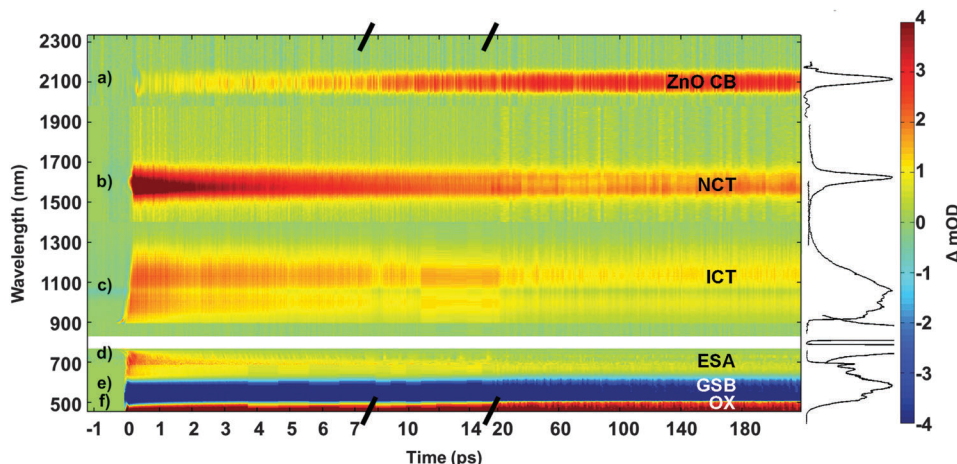
Fig. 1 Ultrafast transient spectra of a DN216/electrodeposited ZnO DSSC in contact with the electrolyte (d–f, also seen for spiroOMeTAD cells) or spiroOMeTAD (a–c). The plotted data are a compilation of four individual example measurements in different spectral regions. (a) and (b) are recorded using a NOPA probe pulse at (2150 ± 20) nm and (1600 ± 20) nm, and (c) and (d)–(f) are recorded using white light continua (900–1300 nm and 450–720 nm), see probe spectra on right of the figure. We plot the change of optical density ΔOD: red signal indicates a newly populated state, while blue signal indicates a bleached state. In order to visualise different time constants the data are plotted with three distinct time scales, as well as assignments of the spectral signals.

infrared NOPA probe pulse, and sections c to f using a WLC probe pulse, see the respective probe pulse spectra on the right edge of the graph. The change in optical density $\Delta OD(\lambda, t)$ is plotted in colour code as a function of the wavelength (vertical) and time (horizontal). A positive change in absorption is shown in red, while a negative change is plotted in blue: newly populated states therefore are shown in red, while depopulated states (bleach) or fluorescence signals, observed by emission stimulated by the probe laser pulse, are shown in blue.

The transient absorption spectrum in Fig. 1 contains several spectral signatures, of which some have been previously assigned to transient states and some not yet: electrons in the ZnO conduction band absorb above 2 μm (section a).[33,34,37–39] The signal centered at around 645 nm corresponds to the excited state absorption (ESA) of the neutral DN216 dye (section d) superimposed to a side band of the oxidised dye absorption (OX),[35,36] 530 nm to its ground state (section e), and 480 nm (the wing of the maximum centered at 440 nm) to the oxidised DN216 (section f) as has been measured spectroelectrochemically.[40] The transient features between 1000 nm and 2000 nm are still to be assigned with help of their temporal evolution: this is achieved by analysing horizontal line outs $\Delta OD(t)$ of the transient spectra in Fig. 2, typically integrated over a range of 20 nm. Some of the characteristic absorption features of different states may overlap spectrally. Therefore the transients are fitted to an appropriate sum of decaying and growing exponential functions and their associated time constants are interpreted independently. The respective amplitudes are not necessarily comparable, since in general the transition probabilities (oscillator strengths) of transient states are unknown. This analysis procedure allows for the deconvolution of the TAS spectrum and enables us to model the ultrafast charge transfer dynamics which occur after photoexcitation of the ZnO/DN216/electrolyte and ZnO/DN216/spiroOMeTAD solar cells, see also ESI.†

Therefore this procedure reveals in detail the processes that take place in the DSSC during conversion of solar energy to electrical energy.

3 Results and discussion

The temporal trace shown in section a in Fig. 1 and 2, taken at $\lambda = 2150 \pm 20$ nm using a NOPA probe pulse will guide us through the analysis and interpretation of all spectral components in Fig. 1 and 2. This transient absorption signal is attributed to free electrons in the conduction band of ZnO.[33,34,37,38] The band gap of ZnO is 3.2 eV (λ_{abs} = 387 nm) and the pump laser pulse at 2.3 eV (λ = 530 nm) only excites the HOMO → LUMO ($S_1 \leftarrow S_0$, 2.3 eV) transition of the DN216 molecules, and therefore these free electrons have been injected from the excited neutral dye molecules into ZnO rather than originating from direct excitation of ZnO.

The fit analysis of the transient signal at 2150 nm reveals that the electron population in the ZnO conduction band grows with three characteristic time constants, an ultrafast $\tau_1 \approx 200$ fs and two slower stepwise processes $\tau_2 = 2$ ps and $\tau_3 = 10$ ps. We will examine these three processes one by one: the ultrafast process reflects a direct electron injection from the vibrationally cold DN216 LUMO into the ZnO conduction band, alike the unhindered injection into nanoporous TiO_2, see also Fig. 3. This interpretation is confirmed by the ultrafast fractional decay of the neutral dye's excited state absorption (ESA) at 675 nm and by an ultrafast increase of the absorption of the oxidised DN216 (OX) at 480 nm, both with the same time constant τ_1, see sections d and f in Fig. 1 and 2, respectively. For each of these electrons directly injected into the ZnO conduction band from the neutral dye's LUMO, one oxidised dye molecule is generated. Data in sections d–f have also been

8940 | *Phys. Chem. Chem. Phys.*, 2016, **18**, 8938–8944

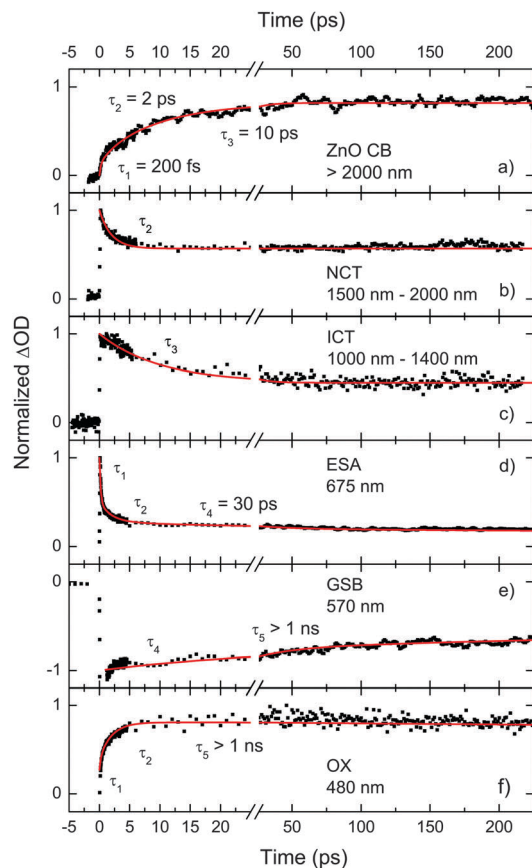This journal is © the Owner Societies 2016

Fig. 2 Temporal evolution of spectroscopic signatures shown in Fig. 1. The line outs (a)–(f) are normalised and correspond to spectral signals in Fig. 1: (a) ZnO conduction band electrons, (b) neutral charge transfer states, (c) ionic charge transfer states, (d) neutral dye's excited state absorption, (e) neutral dye's ground state bleach, and (f) oxidised dye. The photoexcitation of the dye bleaches its ground state (e) and populates the LUMO (d). The excited electron is injected into the ZnO conduction band (a) either directly or via a neutral (b) or an ionic charge transfer state (c), and generates the oxidised dye (f).
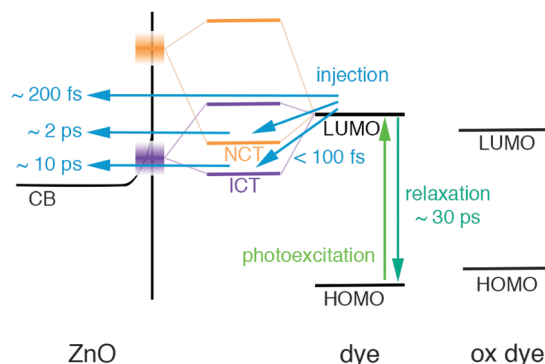

Fig. 3 Schematic representation of energy levels and charge transfer processes taking place upon photoexcitation of a D216/electrodeposited ZnO DSSC in contact with electrolyte or spiroOMeTAD. The favoured injection from the excited dye to the ZnO occurs via three distinct pathways: directly (τ_1 = 200 fs), via a neutral charge transfer state (τ_2 = 2 ps) and via an ionic charge transfer state (τ_3 = 10 ps). As a counter process, intramolecular relaxation also takes place with a time constant of τ_4 = 30 ps.

collected from cells with spiroOMeTAD, and show the same charge dynamics, albeit not as clean due to a developing absorption background in the visible range caused by oxidised spiroOMeTAD in the all solid state cells.[41] Data in traces a and b, on the other hand cannot be collected from electrolyte cells because of the too strong IR absorption of the redox electrolyte. It is therefore indicated that widely identical processes of injection from excited DN216 into ZnO are observed independent of the regenerating contact. This might have been expected since spectral changes as a consequence of regeneration are slower than accessible by the present experiments.[35,36]

The two slower processes populating the conduction band (τ_2 = 2 ps and τ_3 = 10 ps) are interpreted as electron injection from the photoexcited neutral dye (LUMO) into the ZnO conduction band occurring via intermediate states at the dye|ZnO interface. The solar cells studied in this work are made by sensitisation of an electrodeposited highly porous ZnO layer with a monolayer of dye, resulting in almost every excited dye molecule being attached to the ZnO surface. Intermediate

states at the dye|ZnO interface are present as a result of hybrid orbitals generated from the overlap between the neutral dye's LUMO and ZnO surface states known to be present on the surface of electrodeposited highly porous ZnO.[33,34] The indoline dye DN216 is believed to bind to the ZnO surface via its two carboxyl groups,[36] and therefore the same two positions of the dye molecules are attached to the ZnO surface. However, due to the nanostructure of the ZnO surface, a few distinct orbital molecular configurations and, hence, overlap geometries are feasible. According to electron injection time measurements of coumarin dyes on ZnO[33,34] these intermediate states can be molecular dominated if they arise from an overlap of the dye's LUMO with a higher energy ZnO surface state. Their charge and spectral characteristics are then similar to the neutral dye's LUMO and we refer to them as neutral charge transfer states (NCT). Or, they arise from an overlap with a lower energy ZnO surface state, which then dominates the more ionic character of these charge transfer states (ICT), see Fig. 3.

The faster stepwise process (τ_2) is interpreted as injection from the neutral dye's LUMO into the ZnO conduction band via the NCT state, see also Fig. 3. Therefore, in this case, the dye to conduction band electron transfer is a two-step process: a photoexcited electron is injected into the neutral charge transfer state with a time shorter than 100 fs at the limit of our resolution and subsequently into the ZnO conduction band with the slower time constant τ_2 = 2 ps. Due to the similarity of the neutral dye's LUMO and neutral charge transfer state, the first step does not contribute to the decay of the LUMO's absorption signal (ESA), nor to the $\tau_1 \approx$ 100 fs rise of the absorption of the oxidised dye (OX) (section f, Fig. 1 and 2) as electrons are only injected into the neutral charge transfer state. However, a rise in the OX signal and a mirrored decay of the ESA signal with the time constant τ_2 = 2 ps are observed corresponding to electrons injected from the neutral charge transfer state into the ZnO conduction band. This indicates that oxidised dye molecules are only generated because electrons are

transferred out of the molecular dominated intermediate state (NCT) into the conduction band of ZnO. The time scales τ_1 and τ_2 are therefore explained by the complimentary changes in traces a, d and f.

The longer time constant of τ_3 = 10 ps is assigned to the stepwise electron injection into the ZnO conduction band *via* the surface dominated intermediate states (ICT). The initial electron transfer from the photoexcited neutral dye to the ionic charge transfer state occurs on a timescale shorter than 100 fs, at the limit of our temporal resolution. This time constant is observed in both the ESA signal decay and the OX signal rise (sections d and f, Fig. 1 and 2), suggesting that oxidised dye molecules are generated through the initial injection process into the ionic charge transfer states. The second step of the injection pathway, between the ionic charge transfer state and the ZnO conduction band, determines the longer time constant τ_3 = 10 ps. This is again confirmed by τ_3 not being visible in the OX nor ESA signals, as the ionic charge transfer states are most closely related to the ZnO surface states, and the oxidation of dye molecules has already occurred in the first step. All three characteristic times τ_1, τ_2 and τ_3 giving rise to trace a and corresponding changes in d and f can therefore be assigned.

So far, the two distinct charge transfer states (NCT and ICT) have only been indirectly inferred from the dynamics of the LUMO and ZnO CB states. However, in the spectral range from 1000–2000 nm, we find two new, spectrally broad transient absorption bands which we directly assign to the absorptions of the two proposed intermediate states, see Fig. 1 and 2 sections b and c. Both show an instantaneous rise corresponding to the faster than 100 fs injection of the photoexcited electrons from the neutral dye into the intermediate states. Signal b, between 1500–2000 nm decays with the time constant τ_2 = 2 ps (representing injection into the ZnO conduction band) and therefore is assigned to the neutral charge transfer state. The shorter wavelength signal c, between 1000–1400 nm decays with τ_3 = 10 ps and is therefore interpreted as the ionic charge transfer state.

These two charge transfer state signals do not decay to zero. This observation, however, is in perfect agreement with the fact of an overlap with an absorption of oxidised spiroOMeTAD in this spectral range[41] which is thereby shown to decay on a very slow time scale. In contact with the redox electrolyte, signal c correspondingly does decay to zero (signal b cannot be measured in electrolyte contact for experimental reasons as mentioned above). The observation of a rather persistent concentration of oxidised spiroOMeTAD points the attention to a limitation of cell performance by slow hole conduction in the all solid state cells.

A (negative) control measurement was taken using a DN216/Al$_2$O$_3$ film, to confirm that the intermediate charge transfer states were a consequence of the electrodeposited ZnO and not a characteristic of the indoline dye. Therefore for the DN216/Al$_2$O$_3$ film, we have not observed any signal in the near IR region, where the NCT and ICT states have been detected in the DN216/ZnO sample. Other transient absorption measurements taken on indoline dye sensitised Al$_2$O$_3$ solar cells show that they behave similar to indoline dye sensitised ZnO in the visible regime, however no Stark shift is observed.[23,24,32]

Table 1 Summary of spectral signatures of the DN216 dye (neutral and oxidised), the ZnO conduction band and the two charge transfer states as well as their temporal evolutions, as shown in Fig. 1 and 2

Signal	λ/nm	τ/ps	Nature	%
ZnO CB	>2000	0.2	Rise	15
		2	Rise	10
		10	Rise	75
NCT	1500–2000	<0.1	Rise	
		2	Decay	45
		Constant	(Ox spiro)	55
ICT	1000–1400	<0.1	Rise	
		10	Decay	55
		Constant	(Ox spiro)	45
ESA	675	<0.1	Rise	
		0.2	Decay	50
		2	Decay	22
		30	Decay	8
(OX)	>1000		Decay	20
GSB	570 (wing)	<0.1	Depletion	
		30	Repopulation	20
		>1000	Repopulation	80
OX	480 (wing)	<0.1	Rise	15
		0.2	Rise	52
		2	Rise	33
		>1000	Decay	100

Additionally, measurements taken on ZrO$_2$ sensitised solar cells also don't display a Stark shift and electron injection was also found to occur *via* trap states.[31] Note again that for clarity Fig. 1 only displays selected probe ranges. The full range between 900 nm and 2400 nm has, however, been gradually probed by tuning the NOPA probe centre wavelength.

By fitting the ESA signal (section d, Fig. 1 and 2), a further time constant of approximately τ_4 = 30 ps is obtained from the decay of the excited dye's absorption. This is attributed to the non-radiative relaxation of photoexcited neutral dye molecules back to the ground state, since it is also observed as a repopulation time constant in the ground state bleach (GSB) signal (570 nm in the wing of the bleach) of the neutral dye (section e, Fig. 1 and 2). This unwanted relaxation accounts for 20% of the ground state regeneration, while 80% of the photoexcited electrons are injected into the ZnO. Finally, the oxidised dye is reduced with a time constant (τ_5) greater than 1 ns, also mirrored as a repopulation time of the dye's ground state. This dynamics is attributed to the reduction of oxidised dye molecules by the redox couple or spiroOMeTAD, both of which appear to take place on a similar timescale.

All observed spectral signatures and their temporal evolution could be consistently explained in the model, which is summarised and presented in Table 1 and Fig. 3.

4 Conclusions

With the use of transient absorption spectroscopy, we formulated a complete charge transfer model explaining the charge

8942 | *Phys. Chem. Chem. Phys.*, 2016, **18**, 8938–8944

This journal is © the Owner Societies 2016

transfer processes which occur in an indoline dye/electrodeposited ZnO DSSC in contact with the electrolyte or spiroOMeTAD, upon photoexcitation (Fig. 3) resulting in the conversion of light to electrical energy. Electron injection, from the photoexcited neutral dye into the ZnO conduction band, occurs *via* three distinct pathways: direct injection ($\sim$200 fs), injection *via* a neutral charge transfer state, NCT ($\sim$2 ps) and injection *via* an ionic charge transfer state, ICT ($\sim$10 ps). These two distinct charge transfer states were detected as new transient absorption signals between 1000–2000 nm. Due to the nature of the NCT state being most similar to the neutral dye molecule, both the direct injection and the injection from the NCT state into the ZnO conduction band, produce an oxidised dye molecule. Conversely, the injection into the ICT state generates an oxidised dye molecule, while the injection from the ICT state is independent of the generation of oxidised dye molecules. For cell optimisation, ultrafast electron injection times are preferable thus avoiding recombination processes. Since such recombination reactions occur considerably slower, they were not monitored by the present experiments. A persistent concentration of oxidised spiroOMeTAD, however, may indicate the relevance of this loss channel. Direct decay of the excited state of the dye to the ground state $\tau_4 = 30$ ps, however, was directly detected in the present experiments and contributed a 20% loss. While distinct configurations of dye molecules bound to the ZnO surface may play a decisive role in the formation of the different CT states, it is remarkable that these CT states appear to be independent of the iodide/triiodide electrolyte solution or spiroOMeTAD and they seem to exist for different dye molecules[34] and for both, nanostructured and nanoparticulate ZnO surfaces, however not for Al_2O_3 films. Hence, our transient absorption results show that two distinct ZnO surface states are involved in charge transfer from organic molecules into ZnO, and indicate that the existence of these intermediate states is a general property of ZnO.

References

1 M. Grätzel, *Acc. Chem. Res.*, 2009, **42**, 1788–1798.
2 J. M. Ball, M. M. Lee, A. Hey and H. J. Snaith, *Energy Environ. Sci.*, 2013, **6**, 1739–1743.
3 N.-G. Park, *J. Phys. Chem. Lett.*, 2013, **4**, 2423–2429.
4 B. O'Regan and M. Grätzel, *Nature*, 1991, **353**, 737–740.
5 A. Yella, H.-W. Lee, H. N. Tsao, C. Yi, A. K. Chandiran, M. Nazeeruddin, E. W.-G. Diau, C.-Y. Yeh, S. M. Zakeeruddin and M. Grätzel, *Science*, 2011, **334**, 629–634.
6 S. Ferrere, A. Zaban and B. A. Gregg, *J. Phys. Chem. B*, 1997, **101**, 4490–4493.
7 P. Ganesan, A. Yella, T. W. Holcombe, P. Gao, R. Rajalingam, S. A. Al-Muhtaseb, M. Grätzel and M. K. Nazeeruddin, *ACS Sustainable Chem. Eng.*, 2015, 2389–2396.
8 N. Koumura, Z.-S. Wang, S. Mori, M. Miyashita, E. Suzuki and K. Hara, *J. Am. Chem. Soc.*, 2006, **128**, 14256–14257.
9 G. Y. Margulis, B. Lim, B. E. Hardin, E. L. Unger, J.-H. Yum, J. M. Feckl, D. Fattakhova-Rohlfing, T. Bein, M. Grätzel, A. Sellinger and M. D. McGehee, *Phys. Chem. Chem. Phys.*, 2013, **15**, 11306–11312.
10 E. Palomares, J. N. Clifford, S. A. Haque, T. Lutz and J. R. Durrant, *Chem. Commun.*, 2002, 1464–1465.
11 F. Bella, C. Gerbaldi, C. Barolo and M. Gratzel, *Chem. Soc. Rev.*, 2015, **44**, 3431–3473.
12 G. K. Mor, K. Shankar, M. Paulose, O. K. Varghese and C. A. Grimes, *Nano Lett.*, 2006, **6**, 215–218.
13 U. Bach, D. Lupo, P. Comte, J. E. Moser, F. Weissortel, J. Salbeck, H. Spreitzer and M. Grätzel, *Nature*, 1998, **395**, 583–585.
14 J. A. Chang, J. H. Rhee, S. H. Im, Y. H. Lee, H. jung Kim, S. I. Seok, M. K. Nazeeruddin and M. Grätzel, *Nano Lett.*, 2010, **10**, 2609–2612.
15 C.-Y. Hsu, Y.-C. Chen, R. Y.-Y. Lin, K.-C. Ho and J. T. Lin, *Phys. Chem. Chem. Phys.*, 2012, **14**, 14099–14109.
16 D. Stockwell, Y. Yang, J. Huang, C. Anfuso, Z. Huang and T. Lian, *J. Phys. Chem. C*, 2010, **114**, 6560–6566.
17 http://www.nrel.gov/ncpv/images/efficiency_chart.jpg.
18 S. Mathew, A. Yella, P. Gao, R. Humphry-Baker, F. E. Curchod, N. Ashari-Astani, I. Tavernelli, U. Rothlisberger, N. Khaja and M. Grätzel, *Nat. Chem.*, 2014, **6**, 242–247.
19 K. Kakiage, Y. Aoyama, T. Yano, K. Oya, J.-i. Fujisawa and M. Hanaya, *Chem. Commun.*, 2015, **51**, 15894–15897.
20 J. Bouclé and J. Ackermann, *Polym. Int.*, 2012, **61**, 355–373.
21 G. Kumara, J. Tiskumara, C. Ranasinghe, I. Rathnayake, W. Wanninayake, E. Jayaweera, L. Bandara and R. Rajapakse, *Electrochim. Acta*, 2013, **94**, 34–37.
22 J. A. Anta, E. Guillén and R. Tena-Zaera, *J. Phys. Chem. C*, 2012, **116**, 11413–11425.
23 J. Sobuś, G. Burdziński, J. Karolczak, J. Idígoras, J. A. Anta and M. Ziółek, *Langmuir*, 2014, **30**, 2505–2512.
24 J. Sobuś, J. Karolczak, D. Komar, J. A. Anta and M. Ziółek, *Dyes Pigm.*, 2015, **113**, 692–701.
25 J. Idigoras, G. Burdziński, J. Karolczak, J. Kubicki, G. Oskam, J. A. Anta and M. Ziółek, *J. Phys. Chem. C*, 2015, **119**, 3931–3944.
26 P. Tiwana, P. Docampo, M. B. Johnston, H. J. Snaith and L. M. Herz, *ACS Nano*, 2011, **5**, 5158–5166.
27 T. Yoshida, M. Iwaya, H. Ando, T. Oekermann, K. Nonomura, D. Schlettwein, D. Wohrle and H. Minoura, *Chem. Commun.*, 2004, 400–401.
28 Z. Chen, Y. Tang, L. Zhang and L. Luo, *Electrochim. Acta*, 2006, **51**, 5870–5875.
29 S. I. Cha, Y. Kim, K. H. Hwang, Y.-J. Shin, S. H. Seo and D. Y. Lee, *Energy Environ. Sci.*, 2012, **5**, 6071–6075.
30 M. Pagliaro, R. Ciriminna and G. Palmisano, *ChemSusChem*, 2008, **1**, 880–891.
31 K. Oum, P. W. Lohse, O. Flender, J. R. Klein, M. Scholz, T. Lenzer, J. Du and T. Oekermann, *Phys. Chem. Chem. Phys.*, 2012, **14**, 15429–15437.
32 F. Oliver, P. W. Lohse, D. Juan, O. Torsten, S. Mirko, O. Kawon and L. Thomas, *Z. Phys. Chem.*, 2015, **229**, 1907–1928.
33 A. Furube, R. Katoh, K. Hara, S. Murata and M. T. Hironori Arakawa, *J. Phys. Chem. B*, 2003, **107**, 4162–4166.

This journal is © the Owner Societies 2016

Phys. Chem. Chem. Phys., 2016, **18**, 8938–8944 | 8943

34 A. Furube, R. Katoh, T. Yoshihara, K. Hara, S. Murata, H. Arakawa and M. Tachiya, *J. Phys. Chem. B*, 2004, **108**, 12583–12592.

35 E. Rohwer, C. Richter, N. Heming, K. Strauch, C. Litwinski, T. Nyokong, D. Schlettwein and H. Schwoerer, *ChemPhysChem*, 2013, **14**, 132–139.

36 E. Rohwer, I. Minda, G. Tauscher, C. Richter, H. Miura, D. Schlettwein and H. Schwoerer, *ChemPhysChem*, 2015, **16**, 893.

37 J. B. Asbury, E. Hao, Y. Wang, H. N. Ghosh and T. Lian, *J. Phys. Chem. B*, 2001, **105**, 4545–4557.

38 N. A. Anderson, X. Ai and T. Lian, *J. Phys. Chem. B*, 2003, **107**, 14414–14421.

39 J. B. Asbury, Y. Wang and T. Lian, *J. Phys. Chem. B*, 1999, **103**, 6643–6647.

40 J. Falgenhauer, C. Richter, H. Miura and D. Schlettwein, *ChemPhysChem*, 2012, **13**, 2893–2897.

41 H. J. Snaith, R. Humphry-Baker, P. Chen, I. Cesar, S. M. Zakeeruddin and M. Grätzel, *Nanotechnology*, 2008, **19**, 424003.